2019

Petroarchaeometric Data on Antiparos Obsidian (Greece) for Provenance Study by SEM-EDS and XRF

F. Micheletti
Dipartimento di Scienze della Terra e Geoambientali

M. Pallara
Dipartimento di Scienze della Terra e Geoambientali

I. M. Muntoni
Soprintendenza Archeologia

R. H. Tykot
University of South Florida

Original Study

Pasquale Acquafredda*, Francesca Micheletti, Italo Maria Muntoni, Mauro Pallara, Robert H. Tykot

Petroarchaeometric Data on Antiparos Obsidian (Greece) for Provenance Study by SEM-EDS and XRF

https://doi.org/10.1515/opar-2019-0003
Received July 23, 2018; accepted November 16, 2018

Abstract: The island of Antiparos belongs to the Aegean volcanic arc. The obsidian outcrops here contain pieces of excellent tool-making quality, but of small size making the raw material less attractive.Geological samples collected at Soros beach, at Blaco and Mastichi, in the southern part of the island, were analysed using Optical Microscopy, XRF (whole rock) and SEM-EDS (glass and microliths-microphenocrysts). The results obtained demonstrate the potential for distinguishing the Antiparos obsidian from other major central-western Mediterranean sources in an absolutely non-destructive way, using an XRF spectrometer or alternatively with an SEM equipped with an ED spectrometer.

Keywords: Antiparos; obsidian provenance; WD-XRF; SEM-EDS; non-destructive analyses

1 Introduction

The study of obsidian distribution can provide important information on cultural, social and economic relationships between peoples in the Mediterranean during the Neolithic, Copper Age, Bronze Age, and Iron Age. In the past, much data have provided a well-defined outline of the circulation of obsidian from the Mediterranean sources of Monte Arci, Palmarola, Lipari, Pantelleria, Gyali and Melos (Tykot, 2017a) (Fig. 1); the source of Antiparos has been less studied, chiefly because there is no clear evidence of it being traded or exchanged towards the Western Mediterranean, Southeastern Europe, or the Near East region. Recent studies have identified examples of artifacts coming from very far away sources, especially in later time periods, hence the importance of considering all possible sources in archaeological studies (e.g. Ruka et al. 2019; Tykot, 2018).

Article note: This article is a part of Topical Issue on Scientific Studies of Obsidian Sources and Trade, edited by Robert H. Tykot, Maria Clara Martinelli, Andrea Vianello

***Corresponding author: P. Acquafredda,** Dipartimento di Scienze della Terra e Geoambientali - Università degli Studi di Bari 'Aldo Moro', via E. Orabona 4, 70125 Bari, Italy; Centro Interdipartimentale "Laboratorio di Ricerca per la Diagnostica dei Beni Culturali", via E. Orabona 4, 70125 Bari, Italy, E-mail: pasquale.acquafredda@uniba.it
F. Micheletti, M. Pallara, Dipartimento di Scienze della Terra e Geoambientali - Università degli Studi di Bari 'Aldo Moro', via E. Orabona 4, 70125 Bari, Italy
I.M. Muntoni, Soprintendenza Archeologia, Belle Arti e Paesaggio per le Province di Barletta-Andria-Trani e Foggia, via A.A. Valentini 8, 71121 Foggia, Italy
R.H. Tykot, Department of Anthropology, University of South Florida, 4202 E. Fowler Avenue, Tampa, FL 33620, USA

Figure 1. Obsidian source areas of the Mediterranean basin.

Previous research on Antiparos obsidian has characterised these volcanic rocks from a petrographic and geochemical perspective (Innocenti et al., 1982), or to study their artefact provenance in a more or less non-destructive way (Carter & Contreras, 2012; Milić, 2014).

In particular, Antiparos obsidian was characterised with a non-destructive Energy Dispersive X-ray Fluorescence (ED-XRF) by Carter & Contreras (2012), who analysed a large number of geological samples, and by Milić (2014) who analysed only one sample; specifically the ED characterization of Antiparos obsidian by Carter & Contreras (2012, p. 600) was performed in a partially destructive way because the Authors had to prepare "a freshly flaked surface for the X-ray beam, as post-depositional processes have been shown to result in outer cortical or weathered surfaces having diminished concentrations of certain elements, Na in particular, K and Fe to a lesser extent".

Antiparos obsidian has been used on rare occasions by ancient populations and seemingly only by local communities; further information concerning their archaeological use are detailed in Carter & Contreras (2012).

During this research we have produced a new, complementary study because (a) we found a larger area of outcrops than hitherto documented, (b) we used different analytical techniques, (c) we have included comparative analyses with source materials from the Central and Western Mediterranean.

In this paper, 17 obsidian samples collected in the southern part of the island of Antiparos were petrographically and chemically characterised through both destructive and non-destructive techniques using optical and electron microscopy and Wavelength Dispersive (WD) spectrometry. Special attention was paid to the non-destructive technique that in recent years has become particularly widespread among obsidian studies by archaeologists, and especially SEM-EDS and WD-XRF using X-ray peak intensity ratios.

In particular SEM X-ray analysis provides very accurate mapping of the obsidian glass, and permits an easier identification of feldspars, especially the sanidines, allowing accurate microanalyses of the microphenocrysts.

The obsidian data obtained for Antiparos outcrops were compared with other data obtained with similar technique, that is the Scanning Electron Microscopy coupled with Energy Dispersive Spectrometer (SEM-EDS) and the WD-XRF, on other obsidian sources in the Mediterranean sea (Acquafredda et al., 1999; Acquafredda & Paglionico, 2004): the comparison of glass chemistry and of feldspar and pyroxene compositions testify that at least for Monte Arci, Palmarola, Lipari, Pantelleria, Gyali, Melos and Antiparos are possible reliable provenance characterizations using absolutely non-destructive techniques.

Moreover, the use of two different analytical techniques that are absolutely non-destructive allowed us to distinguish the Antiparos obsidians from other Mediterranean and Aegean outcrops, and to organize a database that is sharable with other laboratories for sourcing archaeological obsidians.

2 Materials

The island of Antiparos belongs to the Aegean volcanic arc that extends from the Saronic Gulf through Santorini, Kos, Nisyros and Gyali to Turkey. Almost the entire surface of the island consists of metamorphic rocks of Permian age (Fig. 2), whose succession lithostratigraphy consists of coarse-grained Bt-Ms-gneiss, Ms-gneiss with mylonitic foliation and calcitic or dolomitic marbles, sometimes ankeritized or silicified, also with a cataclasitic texture. The metamorphic basement is covered by a paleosol and by carbonatic rocks in particular calcarenite, calcrete and calcretized calcarenite (Bikel, 2011), whose age varies from Neogene to Quaternary.

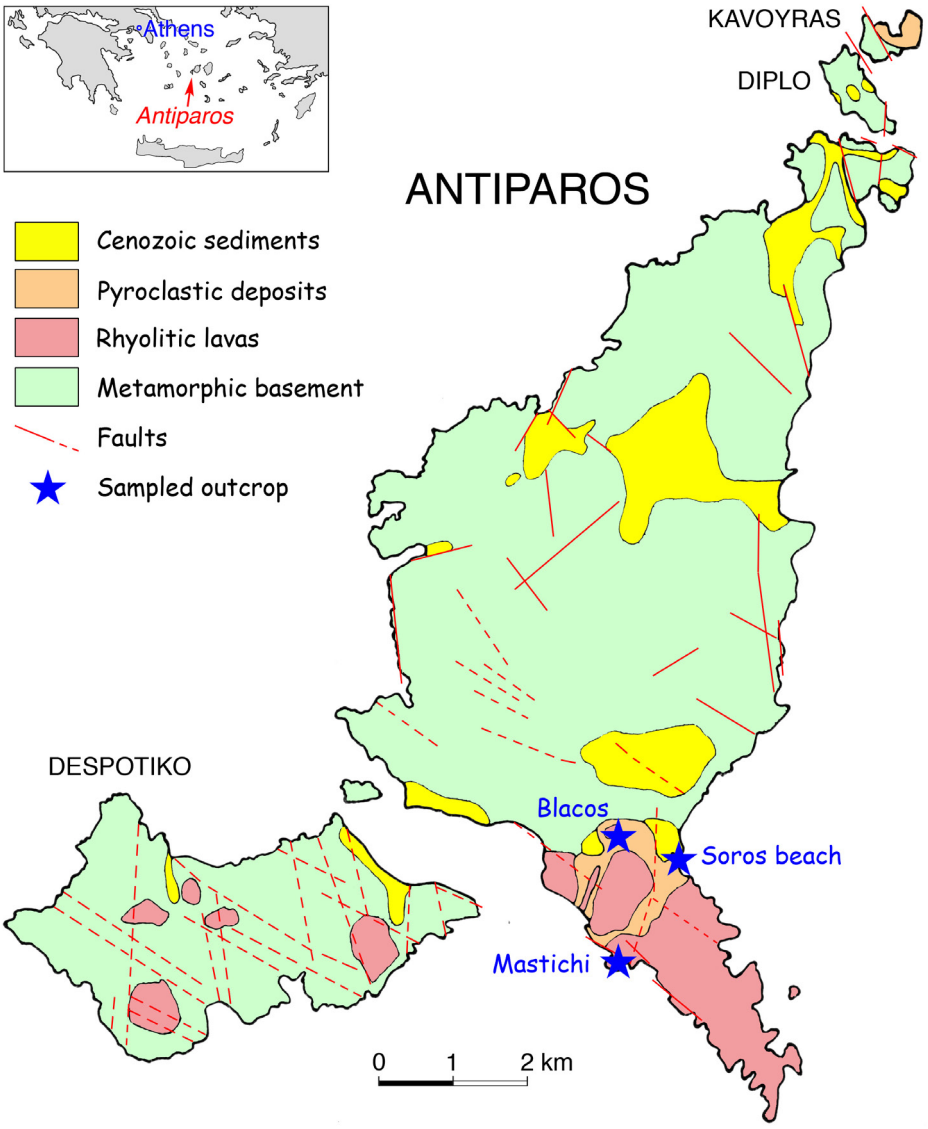

Figure 2. Simplified geological map of Antiparos island (from Innocenti et al., 1982, modified).

Volcanic activity at Antiparos is placed chronologically in the Pliocene: fission track dating of obsidian gave 4.78 Ma (Bigazzi, Bonadonna, & Radi, 1982) and K-Ar dating of unvesiculated vitrophyre rocks suggests ages ranging from 4 to 5.4 Ma (Innocenti et al., 1982); the products of volcanism, interpreted as back-arc rhyolites by Pe-Piper & Piper (2007), are rhyolitic domes, above all rhyolitic lava flows and pyroclastic deposits, that outcrop mainly in the southern part of the island.

The peripheral parts of the domes are often brecciated and associated with volcanic agglomerates. In the southern part of Antiparos lavas are frequently vesiculated with obsidian lenses, also interbedded with white tuff layers. Quaternary tectonic activity also affected the volcanic centres, frequently spreading their outcrops.

A total of 17 obsidian samples were collected in the southern part of the island, in three different locations: Soros beach, Blaco and Mastichi. Six samples (Ant 1, 2, 3, 4, 5 and 6) were collected 500 m west of Soros beach, 60–70 m above sea level, from an outcrop of tuff with embedded fragments of rhyolites and obsidian measuring a few centimeters; another 7 samples (Ant 7, 8, 9, 10, 11, 12 and 13) were collected in the village of Blaco and formed part of rounded nodules containing glass. At Mastichi 4 samples (Ant 14, 15, 17 and 18) were collected: these are obsidian nodules present in the tuffs that flow toward the beach.

3 Analytical Methods

For each sample, a polished thin section was prepared for optical and electron microscope observations; moreover, a representative part of each sample was finely ground for analysis by wavelength dispersive X-ray fluorescence spectrometry (WD-XRF). Finally, a fragment of each sample was extracted to simulate the natural conchoidal fracture of an obsidian artefact to check, once more, the potential for obtaining quantitative chemical data from the natural surface of the obsidian glass as well, as described in Acquafredda et al. (1999) and in Acquafredda & Paglionico (2004).

Petrographic analyses of thin sections were performed using a Zeiss Axioskop 40 POL optical microscope equipped with a Nikon DS-5MC digital camera.

XRF analyses were performed with a PANalytical AXIOS-Advanced XRF spectrometer, equipped with a 4 kW Rh Super Sharp end window X-ray tube. Whole rock obsidian analyses with major and trace element determinations were carried out using powder pellets containing 5 g of finely ground rock treated with 2 cc of a solution containing 15% Elvacite diluted with pure acetone. X-ray intensities were converted into oxide wt. % following the analytical procedure outlined by Leoni & Saitta (1976a, 1976b) and Leoni et al. (2004).

The same PANalytical XRF spectrometer was also used to measure the peak intensity ratio of some trace elements (Rb, Sr, Y, Zr and Nb) under the following operating conditions: 60 kV and 66 mA X-ray tube power supply, using a scintillator detector to collect the X-ray lines dispersed by a LiF 220 crystal (Acquafredda, Muntoni, & Pallara, 2018).

The analysis of the obsidian glass alone was performed both on polished thin sections and raw surfaces of the Antiparos samples using a Zeiss-Leo EVO50XVP scanning electron microscope; the SEM is coupled with an X-max (80 mm^2) silicon drift Oxford detector equipped with a Super Atmosphere Thin Window © for microchemical analyses. Quantitative results were obtained under the following operating conditions: 15 kV accelerating potential, 500 pA probe current, about 25,000 output cps as average count rate on the whole spectrum, counting time 50 s and 8.5 mm working distance. X-ray intensities were converted into concentrations of the element using the XPP correction scheme, developed by Pouchou & Pichoir (1988, 1991), granted as quantitative software support by Oxford-Link Analytical (U.K.). SEM analyses were also carried out on the microcrystals present in the glass: the microanalytical data were checked using numerous reference materials (standards from Micro-Analysis Consultants Ltd.) for mineral phases taking into particular account the crystal chemical formula.

4 Results

Optical microscope petrographic analysis revealed that obsidian from the Antiparos outcrops contains a large number of microphenocrysts presenting a trachytic texture due to the alignment of feldspars and pyroxenes along the lava flow shear zone; the diffused microphenocrysts of feldspars, mainly sanidine (up to 250 μm in size) and subordinate plagioclase (up to 550 μm in size), often present an intersertal or hyalopilitic texture (Fig. 3). Microanalyses of the larger plagioclases show that they are weakly zoned (Table 1).

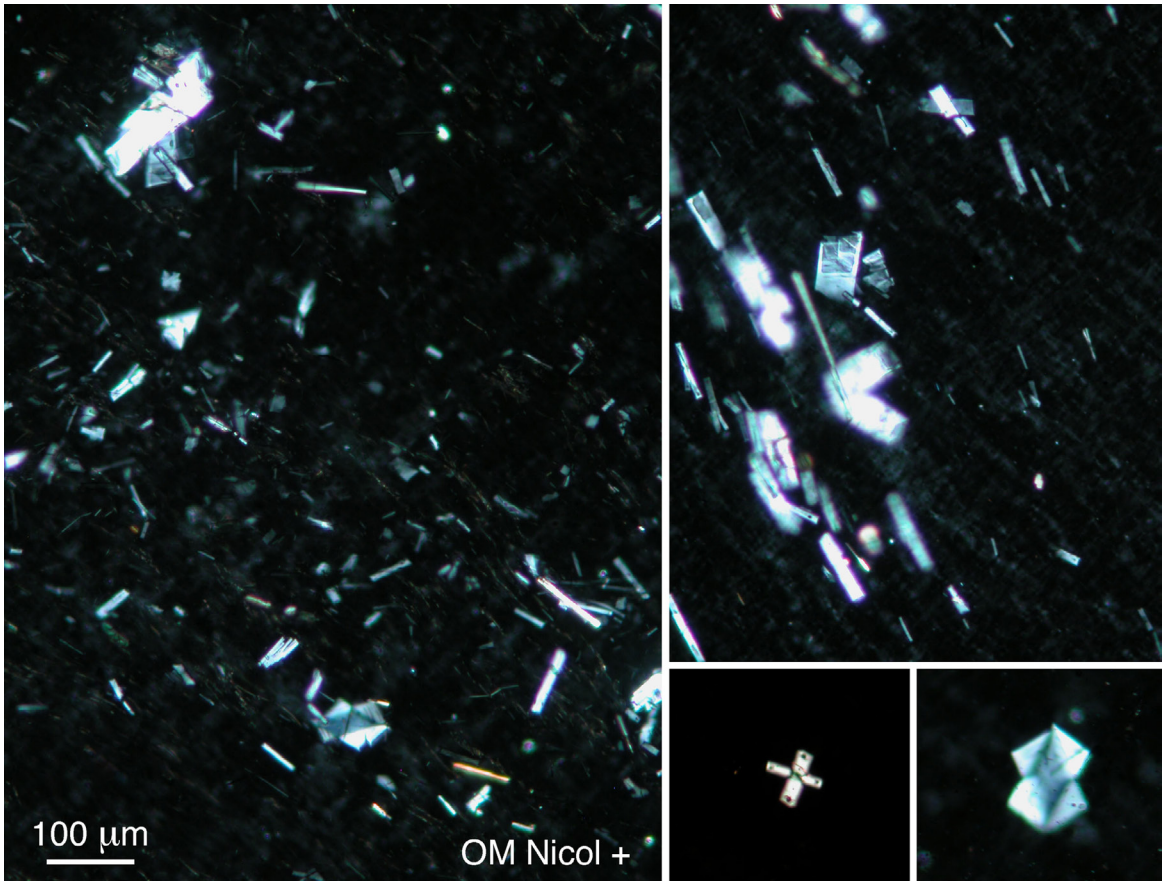

Figure 3. Optical microscope images of a representative sample of Antiparos obsidian (Nicol +); the more widespread microphenocrysts are feldspars, often presenting an alignment along the shear zone due to lava flow (left and top right part of the figure) and hyalopilitic texture (bottom right part of the figure).

The difficulty in distinguishing feldspar, especially sanidine, from the glass of the sample using SEM Back Scattered electron Detector (SEM-BSD) images led to the use of the following procedure for their analysis: 1) a thorough study using light microscopy in which the feldspars were marked using a felt pen on the thin section of the sample; 2) the marked area was observed by SEM X-ray with very accurate mapping (an X-ray acquisition of 20 minutes over an area of 1 mm^2), allowing for an easier identification of feldspars, especially the sanidines (Fig. 4); and 3) the feldspar crystals in this way accurately identified were chemically analysed.

The oligoclasic Antiparos plagioclases are similar in composition to those of Monte Arci (Fig. 4, Table 1); the K-feldspars of Antiparos are sanidines: on average, their composition is more K-rich than that of the alkali feldspars of Pantelleria and Monte Arci (Fig. 4, Table 1). Composition of the feldspars similar to that of Antiparos, ranging from K-rich feldspars to plagioclase, were also signalled by Liritzis et al. (2007) for the Melos geological samples.

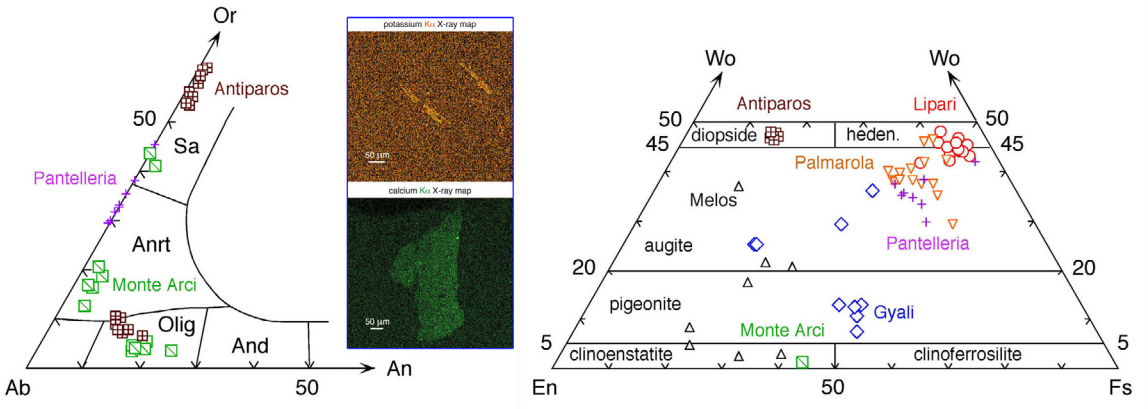

Figure 4. The left-hand diagram shows the composition of the Antiparos feldspars plotted in the Ab-An-Or diagram; Monte Arci and Pantelleria feldspars (data from Acquafredda & Paglionico, 2004) are plotted for comparison. In the blue-bordered inset the X-ray map images used to identify the presence of feldspar crystals: in orange the sanidines (sample Ant 17) and in green the plagioclases (sample Ant 6). The right-hand diagram shows the compositions of pyroxenes according to the Morimoto et al. (1989) nomenclature for the major obsidian source areas in the Mediterranean (Acquafredda & Paglionico, 2004), including the new data from the Antiparos samples. Ab: albite; An: anorthite; Or: orthoclase; Sa: sanidine; Anrt: anorthoclase; Olig: oligoclase; And: andesine; En: enstatite; Fs: ferrosilite; Wo: wollastonite.

Frequent are the microphenocrysts of pale green zoned pyroxene, up to 400 µm in size, that sometimes also present their characteristic basal section (Fig. 5); their diopsidic composition (Fig. 4, Table 2) easily distinguishes them from the pyroxenes of the other Mediterranean sources.

The less frequent amphiboles are pleocroic from pale yellow to pale brown; they measure up to 50 µm in size and often have a skeletal texture (Fig. 5); their composition varies from a Mg-Fe-hornblende to a tschermakitic hornblende. Accessory minerals are opaques, euhedral zircon and more rarely titanite.

WD-XRF analyses provided analytical values (Table 3) that are in line with other data in the literature (Innocenti et al., 1982; Carter & Contreras, 2012) confirming that these rocks have rhyolitic composition. Although the whole rock chemistry of Antiparos obsidian is very similar to those of other geological Mediterranean sources, the major elements of the glass, measured by SEM-EDS, make it possible to differentiate this source from others in the Mediterranean basin (Fig. 6, Table 4). Specifically, the Antiparos samples can be easily differentiated from those of Lipari, Palmarola and Monte Arci using the C.I.A. parameter (Fig. 6); the appreciable spread in the measured values on the raw surfaces results from the difficulties of analysing only the obsidian glass avoiding the frequent feldspar microphenocrysts; these are often too small to be identified even with prior X-ray mapping. Trace elements such as Sr, Y (Fig. 6) and Zr, can quickly distinguish all obsidian sources by using a XRF destructive analytical procedure (Carter & Contreras, 2012).

Alternatively, the Antiparos obsidian can be easily differentiated from the other Mediterranean sources using the WD-XRF peak intensity ratios of trace elements (Fig. 6, Table 5); in fact, in many cases this technique allows for a very good and absolutely non-destructive determination of the source areas (Nelson et al., 1975; De Francesco, Bocci, & Crisci, 2011; Acquafredda et al., 2018) even using samples that are slightly altered or covered by a fine film of carbonate incrustations.

A comparison with the obsidian data regarding the Aegean, Carpathian, central Anatolian, and central Mediterranean sources (Carter & Contreras, 2012; Tykot 2017b) allows asserting that it is possible to distinguish the Antiparos obsidian from those of these sources: this can be performed measuring the trace elements with a destructive technique like WD-XRF on powder pellets; alternatively, the choice to use a non-destructive technique, like the WD-XRF peak intensity ratios of trace elements, necessary to produce for Aegean, Carpathian and Near East obsidians a data base similar to the one of the Mediterranean sources (Acquafredda et al., 2018).

Table 1. Feldspar microanalyses (Pl: plagioclase; San: sanidine) of the Antiparos obsidians; formula on the basis of 8 oxygens. Ab: albite, An: anortite, Or: orthoclase.

Sample	1Ant1	2Ant1	1Ant6a	2Ant6a	3Ant6a	4Ant6a	1Ant11	1Ant3a	1Ant8a	2Ant8a	1Ant17a	1Ant17b	2Ant17b	3Ant17b	4Ant17b	5Ant17b
	Pl	Pl	Pl core	Pl rim	Pl core	Pl rim	Pl	San	San	San	San	San	San	San	San	San
SiO_2	64.89	66.48	65.81	65.30	66.36	65.99	64.09	66.57	66.47	66.30	66.71	67.07	66.78	67.20	65.88	66.36
Al_2O_3	21.43	20.54	20.75	21.51	20.82	21.08	22.07	18.32	18.47	18.96	18.39	18.28	18.10	17.85	18.08	18.47
CaO	2.89	2.32	2.48	2.82	2.13	2.34	3.65	0.25	0.25	0.40	0.25	0.23	0.15	0.14	0.27	0.29
Na_2O	8.98	9.05	9.30	9.19	9.10	9.40	8.88	5.12	4.95	5.09	4.31	4.52	4.84	4.27	4.36	4.56
K_2O	1.39	1.84	1.49	1.31	1.92	1.63	1.19	9.39	9.65	9.33	10.55	10.35	9.69	10.25	10.86	9.99
Total	99.58	100.23	99.83	100.13	100.35	100.44	99.88	99.65	99.79	100.08	100.21	100.45	99.56	99.71	99.45	99.67
Si	2.878	2.927	2.910	2.880	2.919	2.902	2.841	3.013	3.007	2.989	3.013	3.020	3.025	3.041	3.009	3.008
Al	1.120	1.066	1.081	1.118	1.079	1.093	1.153	0.977	0.985	1.008	0.979	0.970	0.966	0.952	0.973	0.987
Ca	0.137	0.109	0.117	0.133	0.100	0.110	0.173	0.012	0.012	0.019	0.012	0.011	0.007	0.007	0.013	0.014
Na	0.772	0.773	0.797	0.786	0.778	0.802	0.763	0.449	0.434	0.445	0.377	0.395	0.425	0.375	0.386	0.401
K	0.079	0.103	0.084	0.074	0.108	0.091	0.067	0.542	0.557	0.537	0.608	0.594	0.560	0.592	0.633	0.578
Σ cat.	4.986	4.978	4.989	4.991	4.984	4.998	4.997	4.993	4.995	4.998	4.989	4.990	4.983	4.967	5.014	4.988
Ab	78.1	78.4	79.8	79.2	78.9	79.9	76.0	44.8	43.3	44.5	37.8	39.5	42.8	38.5	37.4	40.4
An	13.9	11.1	11.8	13.4	10.2	11.0	17.3	1.2	1.1	1.9	1.2	1.1	0.7	0.7	1.3	1.4
Or	8.0	10.5	8.4	7.4	10.9	9.1	6.7	54.0	55.5	53.6	60.9	59.4	56.4	60.8	61.3	58.2

Table 2. Pyroxene microanalyses of the Antiparos obsidians; formula on the basis of 6 oxygens. En: enstatite, Fs: ferrosilite, Wo: wollastonite.

Sample	4Ant 1	6Ant 1	7Ant 1	8Ant 1	11Ant 7	19Ant 15
SiO_2	53.58	53.17	53.39	53.63	53.67	53.54
TiO_2	0.00	0.19	0.12	0.25	0.35	0.25
FeO	9.31	9.04	9.07	9.43	8.98	9.45
Al_2O_3	0.65	0.67	0.86	0.93	0.66	1.11
MnO	2.03	1.98	2.06	1.97	1.90	1.95
MgO	12.28	12.47	12.43	12.02	12.32	12.26
CaO	21.92	22.37	21.99	22.22	22.42	21.63
Total	99.77	99.89	99.92	100.45	100.30	100.19
Si	2.014	1.999	2.003	2.004	2.006	2.002
Ti	0.000	0.005	0.003	0.010	0.010	0.007
Al	0.029	0.030	0.038	0.041	0.029	0.049
Fe^{2+}	0.293	0.284	0.285	0.295	0.281	0.296
Mn	0.065	0.063	0.065	0.062	0.060	0.062
Mg	0.688	0.699	0.695	0.670	0.686	0.684
Ca	0.883	0.901	0.884	0.890	0.898	0.869
Σ cat	3.971	3.981	3.974	3.968	3.970	3.966
En	36.9	37.1	37.3	36.1	36.8	36.8
Fs	15.7	15.1	15.3	15.9	15.1	15.1
Wo	47.4	47.8	47.4	48.0	48.1	47.0

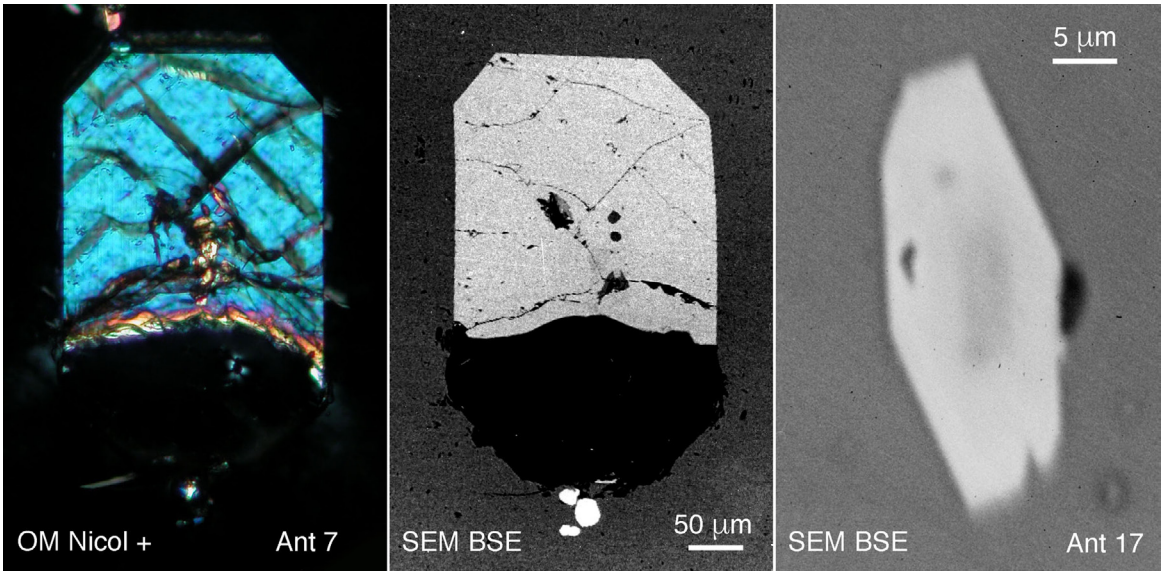

Figure 5. Left and center: Optical microscopy photographs of a diopsidic pyroxene present in the glass of the Antiparos obsidian (sample Ant 7. Nicol +) and the same crystal photographed with the SEM using a back scattered electron detector. Right: image of an amphibole (sample Ant 7. SEM BSE) with skeletal texture.

Table 3. WD-XRF whole rock analyses of Antiparos obsidian; major elements are expressed as oxide weight percent (wt.%) and trace elements as elemental part per million (ppm). Loss on ignition was not determined to permit a better comparison with SEM-EDS analyses.

Sample	SiO_2	TiO_2	Al_2O_3	Fe_2O_3	MnO	MgO	CaO	Na_2O	K_2O	Ba	Rb	Sr	Y	Zr	Nb	V	Cr	Ni	La	Ce
Ant 1	75.71	0.12	12.78	1.11	0.10	0.00	0.46	4.73	4.99	30	440	9	21	152	40	3	58	2	53	64
Ant 2	75.66	0.12	12.78	1.12	0.10	0.01	0.46	4.74	5.00	31	442	9	22	154	41	3	51	2	52	60
Ant 3	75.62	0.12	12.69	1.16	0.10	0.00	0.47	4.68	5.15	29	396	8	16	129	33	2	32	2	50	64
Ant 4	75.78	0.12	12.68	1.12	0.10	0.00	0.44	4.68	5.08	29	433	8	20	147	39	2	30	2	49	60
Ant 5	75.72	0.12	12.74	1.11	0.10	0.00	0.44	4.72	5.05	28	434	8	20	147	39	3	27	2	53	63
Ant 6	75.67	0.12	12.75	1.12	0.10	0.00	0.44	4.75	5.05	32	438	9	21	152	40	2	33	2	52	61
Ant 7	75.65	0.12	12.82	1.11	0.10	0.00	0.44	4.71	5.04	28	429	8	19	141	38	3	34	2	53	62
Ant 8	75.63	0.12	12.70	1.15	0.10	0.00	0.46	4.70	5.14	32	427	8	19	144	38	3	31	2	50	62
Ant 9	75.76	0.12	12.74	1.10	0.10	0.00	0.44	4.73	5.01	27	429	8	19	143	38	2	29	1	52	64
Ant 10	75.67	0.12	12.77	1.13	0.10	0.00	0.45	4.69	5.08	29	413	8	16	135	35	2	37	2	51	62
Ant 11	75.77	0.11	12.72	1.11	0.10	0.01	0.47	4.73	4.99	26	444	7	23	144	41	2	42	2	50	61
Ant 12	75.92	0.11	12.67	1.09	0.10	0.00	0.43	4.69	4.99	23	429	6	18	133	38	2	25	2	49	63
Ant 13	75.75	0.12	12.71	1.11	0.10	0.00	0.43	4.48	5.30	31	437	8	20	152	39	2	27	2	52	62
Ant 14	75.88	0.11	12.64	1.09	0.09	0.20	0.41	4.11	5.48	32	427	9	18	127	37	2	31	2	49	58
Ant 15	75.71	0.11	12.78	1.10	0.10	0.00	0.42	4.64	5.12	31	434	8	19	147	38	2	39	2	55	64
Ant 17	75.79	0.12	12.71	1.12	0.10	0.00	0.43	4.65	5.08	29	427	7	20	142	38	2	39	2	52	60
Ant 18	75.73	0.12	12.72	1.12	0.10	0.00	0.45	4.72	5.05	30	429	8	18	140	38	2	33	2	51	63

Localities of the analysed samples: Soros Beach. Ant 1. 2. 3. 4. 5. 6; Blaco. Ant 7. 8. 9. 10. 11. 12. 13; Mastichi. Ant 14. 15. 17. 18

Table 4. SEM-EDS microanalyses on thin sections (ts) and raw surfaces (rs) of obsidian glass; each value reported in the table represents the mean of three different determinations.

Camp	SiO_2	Al_2O_3	FeO	MgO	CaO	Na_2O	K_2O
Ant 1 ts	74.84	12.70	0.80	0.63	0.40	6.18	4.46
Ant 3 ts	75.43	12.45	0.77	0.50	0.23	6.09	4.54
Ant 5 ts	75.11	12.52	0.70	0.60	0.29	6.29	4.49
Ant 7 ts	75.42	12.54	0.71	0.53	0.25	6.01	4.54
Ant 12 ts	75.51	12.41	0.76	0.55	0.27	6.09	4.41
Ant 15 ts	75.26	12.45	0.69	0.59	0.23	6.19	4.59
Ant 17 ts	75.47	12.44	0.71	0.50	0.27	6.07	4.54
Ant 18 ts	75.42	12.41	0.65	0.52	0.35	6.22	4.44
Ant 1 rs	74.63	12.86	1.01	0.68	0.24	5.48	5.10
Ant 2 rs	75.51	12.41	0.76	0.55	0.27	6.09	4.41
Ant 3 rs	75.50	12.66	0.75	0.53	0.32	4.88	5.35
Ant 4 rs	74.70	12.61	0.65	0.72	0.26	6.65	4.41
Ant 5 rs	76.35	12.14	0.92	0.35	0.34	4.72	5.18
Ant 6 rs	74.51	12.80	0.72	0.70	0.23	6.65	4.38
Ant 7 rs	75.22	12.55	0.74	0.60	0.30	5.67	4.92
Ant 8 rs	75.40	12.41	0.78	0.57	0.38	5.70	4.77
Ant 9 rs	75.10	12.62	0.67	0.63	0.21	5.20	5.57
Ant 10 rs	75.31	12.57	0.59	0.61	0.26	6.35	4.32
Ant 11 rs	75.56	12.41	0.71	0.56	0.23	6.17	4.36
Ant 12 rs	76.58	12.52	0.55	0.11	0.27	5.49	4.47
Ant 13 rs	75.21	12.58	0.78	0.65	0.26	5.13	5.40
Ant 15 rs	74.91	12.64	0.63	0.67	0.31	6.39	4.44
Ant 17 rs	76.45	12.75	0.69	0.57	0.21	4.77	4.56
Ant 18 rs	75.40	12.83	0.69	0.78	0.32	5.84	4.14

Table 5. X-ray emission and characterizing ratio of some contiguous trace elements of Antiparos obsidian. The X-rays intensity values. expressed as counts per second. are background and interference free.

	Rb	Sr	Y	Zr	Nb	Rb/Sr	Zr/Y	Zr/Nb	Nb/Y	Nb/Sr	Y/Nb
Ant 1	38656.5	868.5	2048.1	19763.0	5481.9	44.51	9.65	3.61	2.68	6.31	0.37
Ant 2	38892.0	920.4	2147.5	20048.0	5574.4	42.25	9.34	3.60	2.60	6.06	0.39
Ant 3	34903.0	829.6	1537.9	16728.0	4602.6	42.07	10.88	3.63	2.99	5.55	0.33
Ant 4	38042.0	807.1	1937.1	19061.4	5345.1	47.13	9.84	3.57	2.76	6.62	0.36
Ant 5	38177.4	857.3	1971.0	19135.5	5346.8	44.53	9.71	3.58	2.71	6.24	0.37
Ant 6	38499.1	872.7	2067.1	19824.5	5466.0	44.11	9.59	3.63	2.64	6.26	0.38
Ant 7	37821.6	852.4	1826.4	18424.7	5182.3	44.37	10.09	3.56	2.84	6.08	0.35
Ant 8	37681.9	860.6	1862.4	18766.9	5198.2	43.78	10.08	3.61	2.79	6.04	0.36
Ant 9	37826.4	834.0	1839.9	18615.8	5207.0	45.35	10.12	3.58	2.83	6.24	0.35
Ant 10	36062.7	820.9	1605.4	17637.6	4800.6	43.93	10.99	3.67	2.99	5.85	0.33
Ant 11	39230.8	673.9	2240.0	18807.0	5690.5	58.21	8.40	3.30	2.54	8.44	0.39
Ant 12	37661.8	670.0	1791.8	17358.3	5204.1	56.21	9.69	3.34	2.90	7.77	0.34
Ant 13	38258.2	870.1	2035.5	19685.0	5393.2	43.97	9.67	3.65	2.65	6.20	0.38
Ant 14	37789.9	883.0	1688.4	16432.5	5080.7	42.80	9.73	3.23	3.01	5.75	0.33
Ant 15	38183.8	850.1	1883.5	19093.9	5241.7	44.92	10.14	3.64	2.78	6.17	0.36
Ant 17	38185.0	796.6	1899.7	18449.1	5315.6	47.93	9.71	3.47	2.80	6.67	0.36
Ant 18	37410.8	827.4	1785.7	18286.9	5144.7	45.21	10.24	3.55	2.88	6.22	0.35

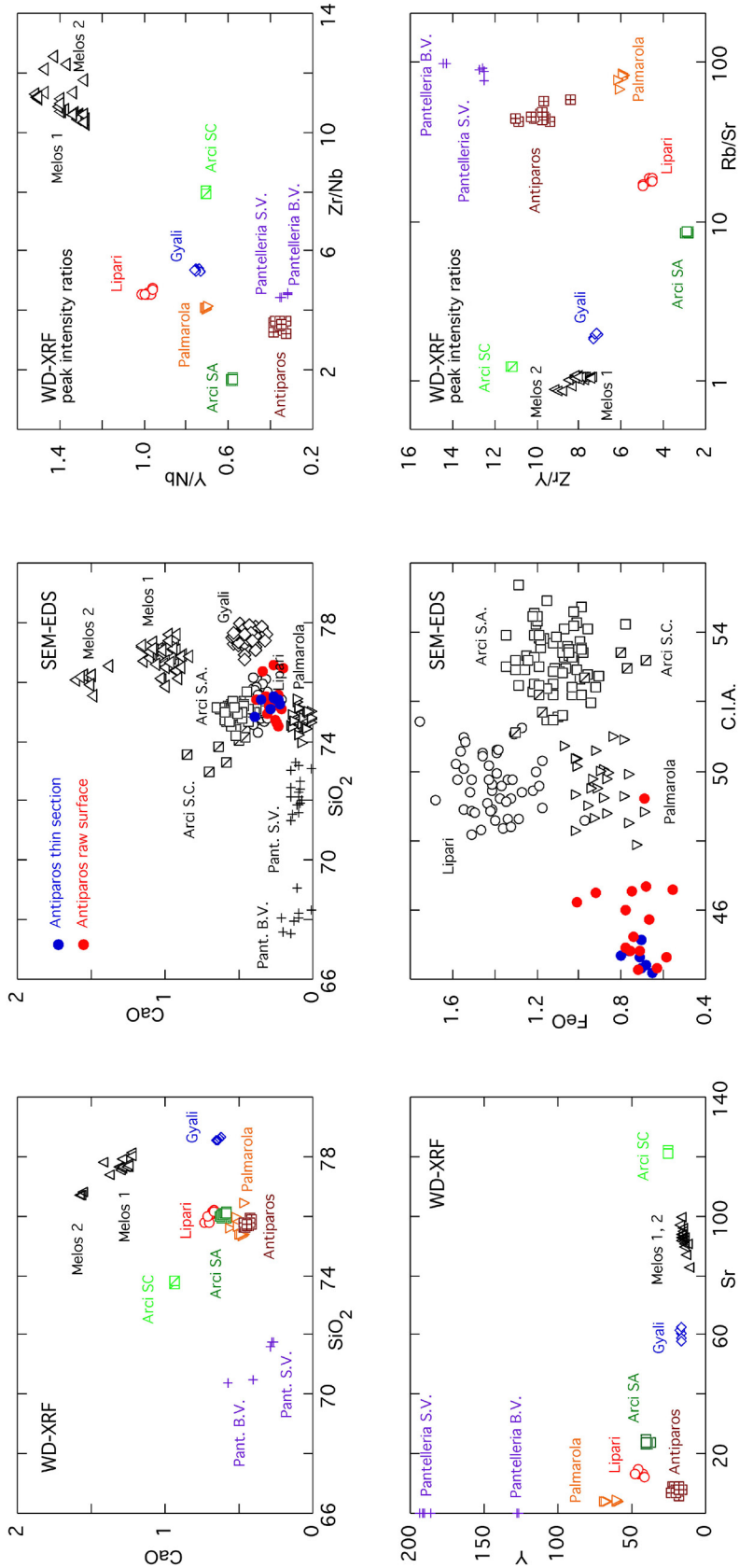

Figure 6. Plots on the left side: WD-XRF data plots of Antiparos obsidian compared with the data from other source areas in the Mediterranean (data from Acquafredda et al., 1999). Plots at the center: SEM-EDS microanalyses of the major obsidian source areas in the Mediterranean basin (data from Acquafredda et al., 1999); Antiparos glass analyses, representing the mean value of at least three microanalyses, are plotted as blue circles (measurements on thin sections) and as red circles (measurements on the equivalent raw surface). Plots on the right side: WD-XRF peak intensity ratios of trace elements that make it possible to differentiate the Antiparos samples from the other Mediterranean source areas (Acquafredda et al., 2018) with a non-destructive technique.

5 Conclusions

Obsidian samples collected in the southern part of the island of Antiparos (Greece) were petrographically and chemically characterised to improve the Mediterranean database used for obsidian provenance attribution. Their whole rock WD-XRF chemical analyses on powder pellets, a destructive technique, furnish a database of major and trace elements; these measures help in comparing the WD-XRF data with the data collected on obsidian artefacts using other non-destructive analytical techniques such as SEM-EDS microanalyses, portable X-ray fluorescence, inductively-coupled plasma mass spectrometry with laser ablation, neutron activation analysis and particle induced X-ray emission. Specifically, during this study the Antiparos obsidian was also characterised with an absolutely non-destructive technique by analysing the glass of the samples with an energy dispersive spectrometer coupled to a scanning electron microscope; these techniques, coupled with very accurate X-ray mapping of the obsidian glass, also made it possible to characterise the chemistry of the microphenocrysts diffusely present in the glass. The SEM-EDS chemical data for the glass are well in line with the data obtained by WD-XRF during this study and other data obtained with the destructive technique present in the literature (Carter & Contreras, 2012).

Finally, the Antiparos samples were also analysed with the X-ray fluorescence technique using peak intensity ratios of trace elements. This provides highly reliable data for samples whose surface is altered, particularly affecting the alkali cations, or covered with a thin film of carbonate encrustations (Acquafredda & Muntoni, 2008; Acquafredda, Muntoni, & Pallara, 2013; Acquafredda et al., 2018).

The optical and electron microscope petrographic and chemical data, also supported by the WD-XRF analysis of Antiparos samples, considerably expand the database for this obsidian source, allowing one to discriminate Antiparos obsidian from neighbouring Aegean obsidians, and to distinguish it from Central and Western Mediterranean raw materials; the minor use of Antiparos obsidians makes it less likely that these rocks circulated widely during the Neolithic (Carter & Contreras, 2012).

Acknowledgments: SEM-EDS analyses were performed with a SDD detector of "Laboratorio per lo Sviluppo Integrato delle Scienze e delle TEcnologie dei Materiali Avanzati e per dispositivi innovativi (SISTEMA)" from the University of Bari.

References

Acquafredda, P., Andriani, T., Lorenzoni, S., & Zanettin, E. (1999). Chemical characterization of obsidians from different Mediterranean sources by non-destructive SEM-EDS analytical method. *Journal of Archaeological Science*, 26, 315–325.

Acquafredda, P. & Paglionico, A. (2004). SEM-EDS microanalyses of microphenocrysts of Mediterranean obsidians: a preliminary approach to source discrimination. *European Journal of Mineralogy*, 16, 419–429.

Acquafredda, P. & Muntoni, I.M. (2008). Obsidian from Pulo di Molfetta (Bari, Southern Italy): provenance from Lipari and first recognition of a Neolithic sample from Monte Arci (Sardinia). *Journal of Archaeological Science*, 35, 947–955.

Acquafredda, P., Muntoni, I.M., & Pallara, M. (2013). SEM-EDS and XRF characterization of obsidian bladelets from Portonovo (AN) to identify raw material provenance. *Origini*, 35, 69–82.

Acquafredda, P., Muntoni, I.M., & Pallara, M. (2018). Reassessment of WD-XRF method for obsidian provenance shareable databases. *Quaternary International*, 468, 169–178.

Bigazzi, G., Bonadonna, F.P., & Radi, G. (1982). Fission track dating of obsidian and prehistory. In *Workshop Track Dating, Abstracts of the Fifth International Conference on Geochronology, Cosmochronology and Isotope Geology* (pp. 1–4). Nikko National Park: Japan.

Bikel, L. (2011). The Quaternary sediments of NW-Antiparos (Aegean): Lithostratigraphy and depositional environment. Master's thesis (Masterarbeit), University of Vienna: Austria.

Carter, T. & Contreras, D.A. (2012). The character and use of the Soros hill obsidian source, Antiparos (Greece). *Comptes Rendus Palevol*, 11, 595–602.

De Francesco, A.M., Bocci, M., & Crisci, G.M. (2011). Non-destructive applications of wavelength XRF in obsidian studies. In M.S. Shackley (Ed.), X-Ray Fluorescence Spectrometry (XRF) in Geoarchaeology (pp. 81–107). Heidelberg: Springer.

Innocenti, F., Kolios, N., Manetti, P., Rita, F., & Villari, L. (1982). Acid and basic late neogene volcanism in central Aegean Sea: Its nature and geotectonic significance. *Bulletin Volcanologique*, 45(2), 87–97.

Leoni, L., Menichini, M., & Saitta, M. (2004). Ricalibrazione di una metodologia in fluorescenza-X per l'analisi di minerali e rocce su campioni di polvere. *Atti della Società Toscana di Scienze Naturali, Memorie*, 109, 13–20.

Leoni, L. & Saitta M. (1976a). X-ray fluorescence analysis of 29 trace elements in rock and mineral standards. *Rendiconti della Società Italiana di Mineralogia e Petrologia*, 32 (2), 497–510.

Leoni, L. & Saitta, M. (1976b). Determination of yttrium and niobium on standard silicate rocks by X-ray fluorescence analyses. *X-ray Spectrometry*, 5, 29–30.

Liritzis, I., Stevenson, C.M., Novak, S.W., Abdelrehim, I., Perdikatsis, V., & Bonini, M. (2007). New prospects in obsidian hydration dating: an integrated approach. In *Proceedings of the Hellenic Archaeometry Society, Athens* (pp. 9–22). British Archaeological Reports (BAR) International Series.

Milić, M. (2014). PXRF characterisation of obsidian from central Anatolia, the Aegean and central Europe. *Journal of Archaeological Science*, 41, 285–296.

Morimoto, N., Fabries, J., Ferguson, A.K., Ginzburg, I.V., Ross, M., Seifert, F.A., Zussman, J., Aoki, K., & Gottardi, G. (1989). Nomenclature of pyroxenes. *Canadian Mineralogist*, 27, 143–156.

Nelson, D.E., D'auria, J.M., & Bennett, R.B. (1975). Characterization of Pacific Northwest coast obsidian by X-ray fluorescence analysis. *Archaeometry*, 17, 85–97.

Pe-Piper, G. & Piper, D.J.W. (2007). Neogene backarc volcanism of the Aegean: New insights into the relationship between magmatism and tectonics. *Geological Society of America Special Papers*, 418, 17–31.

Pouchou, J.L. & Pichoir, F. (1988). A simplified version of the "PAP" model for matrix corrections in EPMA. In D.E. Newbury (Ed.), *Microbeam Analysis* (pp. 315–318). San Francisco Press.

Pouchou, J.L. & Pichoir, F. (1991). Quantitative analysis of homogeneous or stratified microvolumes applying the model "PAP". In K.F.J. Heinrich & D.E. Newbury (Eds.), *Electron Probe Quantitation* (pp. 31–75). Plenum Press: New York.

Ruka, R., Galaty, M., Riebe, D., Tykot, R.H., Gjipali, I., & Kourtessi-Philippakis, G. (2019). pXRF analysis of obsidian artifacts from Albania: Crossroads or cul-de-sac? *Journal of Archaeological Science: Reports,* 24, 39–49.

Tykot, R.H. (2017a). Obsidian studies in the prehistoric central Mediterranean: after 50 years, what have we learned and what still needs to be done? *Open Archaeology*, 3, 264–278.

Tykot, R.H. (2017b). A decade of portable (hand-held) X-ray fluorescence spectrometer analysis of obsidian in the Mediterranean: many advantages and few limitations. *MRS Advances*, 2 (33–34), 1769–1784.

Tykot, R.H. (2018). Obsidian Artifacts: Origin of the Raw Material. In: Forenbaher, S., *Special Place, Interesting Times: The Island of Palagruža and Transitional Periods in Adriatic Prehistory* (pp. 84–87). Archaeopress.